# Molecular dynamics simulation of the formation of W-centers in silicon by Ga ion irradiation

Christos Gennetidis * and Patrice Chantrenne
*INSA-Lyon, Université Claude Bernard Lyon 1, CNRS, MATEIS, UMR 5510, 69621 Villeurbanne, France*

Thomas Wood
*INSA-Lyon, Ecole Centrale de Lyon, Université Claude Bernard Lyon 1, CPE Lyon, CNRS, INL, UMR 5270, 69621 Villeurbanne, France*

(Received 1 November 2023; revised 18 January 2024; accepted 26 January 2024; published 22 February 2024)

Silicon-emitting centers constitute promising candidates for quantum telecommunication technologies. Their operation depends on the fabrication of light-emitting defect centers such as the tri-interstitial Si complex, the W-center. In this paper the formation of Si tri-interstitial clusters after Ga ion beam bombardment on pure silicon substrates and a subsequent annealing stage is investigated using molecular dynamics simulations. This study aims to understand the dynamic formation process of W-centers after Ga irradiation and annealing in order to facilitate their creation using focused ion beam and annealing experimental systems. A tri-interstitial cluster identification method is proposed which considers the configuration of the clusters in the Si lattice in order to identify the defects which will act as candidates for the W-center. This method successfully identifies W-center defect candidates in an ideal system. The number of tri-interstitial clusters increases and spreads deeper into the Si for higher energies and their probability of generation increases until a limiting Ga fluence. Furthermore annealing can eliminate a lot of the unwanted defects maintaining at the same time the number of the tri-interstitial clusters, leading to isolated clusters with less distorted local environment.

DOI: 10.1103/PhysRevB.109.075428

## I. INTRODUCTION

Single-photon emitter technology has drawn the attention of researchers in recent years due to its application in various fields, including quantum telecommunications. From a plethora of candidate materials capable of hosting single-photon emitters, silicon constitutes a material with a wide range of advantages. It may host a large number of point-defect-based emitters such as the G- and W-centers, which incorporate energy levels inside the band gap and emit in or near the telecommunication wavelength bands [1]. Furthermore, silicon is a well-known material which can be integrated into Si microelectronics devices. This, combined with its natural abundance and high purity, makes silicon an important candidate material for quantum applications [2].

The W silicon-emitting center (SEC) is a promising defect which has not been investigated extensively yet. It consists of a Si self-tri-interstitial cluster which demonstrates a trigonal $C_{3v}$ symmetry with its $C_3$ axis parallel to the $\langle 111 \rangle$ crystallographic directions, as was revealed by uniaxial stress measurements carried out by Davies *et al.* [3]. The precise structure of the W-center is still under debate. The I3-I structure consists of three interstitials in an equilateral triangle in a {111} plane bridging three adjacent bond-centered sites [4], whereas the I3-V structure is a wider configuration of the I3-I [5,6]. Both exhibit the $C_{3v}$ symmetry and local vibrational mode energy at 70 meV [6,7]. However, recently Baron *et al.* [7] showed by density functional theory (DFT) simulations that the I3-V defect can account for an optically active W-center whereas the I3-I cannot.

One way to fabricate these defects is the employment of focused ion beam (FIB) irradiation, which can incorporate the desired defects inside the bulk material at a defined depth and high lateral resolution. FIB has been employed to fabricate the silicon vacancy center in diamond [8] and G- and W-centers in silicon with the use of a Si beam [9]. Whether FIB irradiation or wafer-scale irradiation are used, subsequent annealing stages have been shown to annihilate a lot of the damage created during the irradiation and isolate the desired defects which will act as potential photon-emitting centers [3,7–13]. A popular ion beam element in FIB systems is gallium, due to its low vaporization temperature, which, due to its high mass, can lead to a large amount of damage in the irradiated substrate. It is widely used for transmission electron microscopy sample preparations [14–16]. In this applicative domain, molecular dynamics (MD) simulations have been employed to investigate the FIB milling process under different experimental conditions to study the amorphization of the sample [14,16–19]. Furthermore, Xiao *et al.* [20] studied, using MD simulations, the damage formation during the Ga irradiation of Si, as well as the damage evolution after high-temperature annealing, but they did not focus on the formation of any specific kind of defect.

MD simulations are a useful tool to help elucidate the dynamic formation process of different defect centers during the FIB irradiation and subsequent annealing stages. This is its main advantage over other simulation methods such as the binary collision approximation (BCA) method of SRIM

*Corresponding author: christos.gennetidis@insa-lyon.fr

 

software [21]. SRIM is parametrized with experimental irradiation data, so it can calculate with good accuracy the mean stopping depth of the ions. On the other hand, because it treats the lattice as amorphous, it cannot investigate dynamic processes at different temperatures such as the annealing nor can it identify complex defect structures in a crystal lattice such as a tri-interstitial cluster, which is the origin of the W SEC.

Several studies employed MD simulations to investigate different potential single-photon emitting defects after irradiation, especially on SiC [22–24] and diamond [25–27]. Fan *et al.* [23] used H ion irradiation whereas in Ref. [22] they used dual ion irradiation of He and Si to investigate the formation and evolution of Si vacancy defect centers under different annealing conditions. Fu *et al.* [26] irradiated carbon diamond with Si and used annealing at different temperatures in order to create Si vacancy centers. Regarding the Si system, Aboy *et al.* [28] used MD simulations to investigate the formation and evolution of small Si self-interstitial clusters after placing a number of interstitial Si atoms close to each other and annealing the system for 25 ns at 1200 K. Using the Tersoff 3 interatomic potential [29] to account for the Si-Si interactions they observed the formation of the I3-V defect but they did not find the I3-I defect. So far there is neither an experimental nor computational work investigating the formation process of W-centers during Ga ion irradiation on silicon.

In this work, the formation of W-center candidates during the irradiation of Si substrates with Ga atoms and a subsequent annealing stage was investigated by the use of MD simulations. A W-center candidate identification method was developed which takes into account the position and symmetry of the defect which, according to the literature [4–7], constitutes a W-center. Different irradiation energies and fluences compatible with the FIB process as well as different annealing temperatures and times were studied. This investigation aims to understand the formation and evolution process of W-centers under the different experimental conditions.

## II. METHODS

The molecular dynamics simulations were carried out using the LAMMPS [30] simulation software. The interatomic interactions were described by the Tersoff [31] potential smoothly connected with the universal ZBL (Ziegler-Biersack-Littmark) screened nuclear repulsion potential to account for the high-energy collisions between the atoms. During the Ga-Si interactions only the nuclear stopping (elastic collisions) from the ballistic collisions was taken into account. The electronic stopping from inelastic collisions of the atoms with the electrons is considered to have minor impact on slow-moving heavy atoms such as Ga [32]. The potential parameters employed in this work for Si-Si and Ga-Ga can be seen in Refs. [31,33]. The mixing rules [31] have been used to determine the parameters for Ga-Si interactions.

The simulation model consists of a Si atom box and Ga atoms randomly initialized 1 nm above the (001) plane of Si in order to impinge on it with a zero incidence angle to the (001) plane normal. Four Ga beam energies were investigated (0.5 keV, 1 keV, 2 keV, and 5 keV) which are consistent with the low-energy operation of FIB hardware. Two system sizes were used: a small one (217 800 atoms) for the 0.5 keV, 1 keV, and 2 keV energies and a bigger one (579 200 atoms) for the 5 keV energy. Figure 1 depicts the small-size model where the bottom atoms (brown) are fixed and the rest of the atoms (yellow) are free to move under Newtonian interactions with periodic boundary conditions across the $x$ and $y$ directions. One Ga atom at a time is incident in a square region of $10 \times 10$ nm and the system is thermalized at 300 K between each atom's arrival. The irradiation process was divided into two parts. In the first, each Ga atom arrival starts with a time step of 0.02 fs and NVE ensemble to follow the high-energy atom movements and allow the cascade to form naturally. The first part lasts 0.4 ps which is enough for the Ga atom to transfer its energy to the Si lattice. This is within the 0.1–1 ps timescale of the ballistic collision processes [34], where the high-energy collisions between the atoms occur. In the second part the NVT thermostat was used on the whole system with a time step of 0.5 fs for 20 ps to slowly cool down the system back to 300 K.

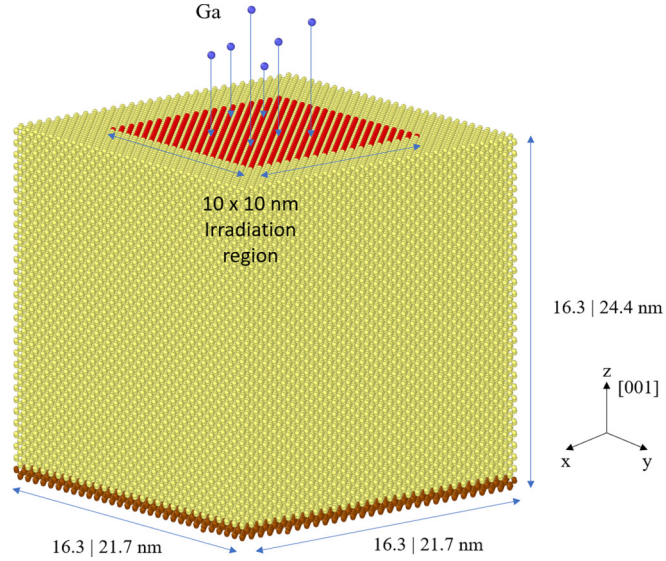


FIG. 1. MD model of irradiation. Blue atoms correspond to the irradiated Ga atoms, brown atoms to the bottom fixed layer, yellow atoms to the Newtonian region, and the red atoms to the surface atoms where the irradiation occurs. The different lengths at the sides indicate the side lengths of the different models employed in this study. Figure created with OVITO software [35].

After the irradiation process the systems were annealed at different temperatures and for different times. Before each annealing the structure was equilibrated at 300 K and zero pressure (NPT) for 50 ps. Then the systems were heated with a heating rate of 0.02 K $fs^{-1}$ to the desired annealing temperature, with a time step of 0.2 fs. After the annealing the system was quenched at the same rate to 300 K where it was thermalized for 50 ps under NPT followed by a 100 ps stage under the NVE ensemble. The average number of defects reported in the following sections was calculated using the methods described below, every 5 ps at this final NVE stage.

The Wigner-Seitz (WS) analysis cannot properly locate all the tri-interstitial clusters, especially those which, according

TABLE I. Vacancy, Si self-interstitial (I1), and tri-interstitial cluster (I3) formation energies in eV, calculated in this work using MD simulations and compared with results from the literature using the DFT local density approximation (LDA), the DFT generalized gradient approximation (GGA PW91), the DFT Heyd-Scuseria-Ernzerhof functional (HSE), as well as the highly accurate diffusion Monte Carlo approach (DMC). The formation energy of I1 in three different configurations was calculated as well as that of the tri-interstitial cluster in the I3-I and I3-V configurations.

| Defect | MD | LDA | GGA | HSE | DMC |
|---|---|---|---|---|---|
| Vacancy | 3.70 | 3.46 [36] | 3.60 [36] | | |
| I1-split-⟨110⟩ | 4.44 | 3.43 [37] | 4.03 [37] | 4.64 [37] | 4.94 [37] |
| I1-hexagonal | 4.54 | 3.62 [37] | 4.23 [37] | 4.82 [37] | 5.13 [37] |
| I1-tetrahedral | 3.58 | 3.56 [37] | 4.21 [37] | 4.92 [37] | 5.05 [37] |
| I3-I | 9.22 | 7.78 [6] | 7.50 [28] | 8.17 [7] | |
| I3-V | 10.51 | 6.88 [6] | 6.74 [28] | 7.52 [7] | |

to the literature [4–7], are more probable to act as an optically active W-center. Thus, an identification method was developed using Python programming alongside the OVITO WS analysis [35] to identify the best candidates for the W-center. First, the WS analysis was employed to select clusters that have atoms which are recognized as interstitials. Then all the clusters in between the {111} planes, which have a maximum distance between their atoms of 3.5 Å, as described later, were located. This distance was found to be sufficient to identify the desired clusters (Sec. III A). Afterward, the ones for which the normal to the plane containing the atoms formed an angle of less than 10 degrees with the ⟨111⟩ directions were selected. This way, the best tri-interstitial candidates for the W-center were selected which will be referred simply as tri-interstitial clusters. Furthermore, this method has the capability to identify from these candidates the ones with the appropriate trigonal symmetry by calculating the interior angles of the tri-interstitial clusters. The symmetric clusters were selected by finding the ones for which the three interior angles did not differ by more than 10 degrees. These clusters will be referred to as symmetric tri-interstitial clusters.

## III. RESULTS AND DISCUSSION

### A. Ideal W-centers

In this section, the formation of a tri-interstitial cluster which can account for a W-center, whose structure is defined according to the literature, Refs. [4–7], is investigated. First, to determine the accuracy of the interatomic potential, the formation energy of a vacancy and a Si self-interstitial in different configurations was calculated. The results alongside a comparison with DFT and diffusion Monte Carlo (DMC) values from the literature [36,37] can be seen in Table I. The formation energies using the MD simulations have a good agreement with the DFT and DMC, which means that the employed potential can effectively reproduce the vacancies and interstitials during the irradiation process. Afterward, the formation energies of two W-center candidates were calculated. In a small Si box of $9 \times 9 \times 9$ lattice constants and 5832 atoms with periodic boundary conditions across each direction a distorted tri-interstitial cluster was placed in between the {111} planes. Afterward, the structure was minimized to find its ground state, and two configurations that resemble the I3-I and I3-V structures of the literature were found [Fig. 2(a)]. The formation energies are 9.2 eV and 10.5 eV for the I3-I and I3-V structures, respectively, meaning that I3-I is the most stable configuration for the employed potential. In general, the Tersoff potential overestimates the formation energies of the tri-interstitial clusters compared with DFT results (Table I). This overestimation is relatively small for the I3-I (1.05 eV to 1.72 eV) and higher for the I3-V (2.99 eV to 3.77 eV) configurations, which might lead to a small underestimation of the total number of tri-interstitial clusters. These structures were annealed at 300 K to investigate their stability. The I3-I defect remained stable, fluctuating around its initial position due to the thermal movements, with the tri-interstitial atoms having a distance of around 2.4 Å [Fig. 2(b)]. The I3-V defect exhibits a small rotation and the distance between the tri-interstitial atoms falls from 3.8 Å at 0 K to 3.4 Å at 300 K [Fig. 2(b)]. In any case they appear to preserve their trigonal symmetry and positioning at 300 K, which validates the use of the employed interatomic potential. Furthermore, the developed method can successfully locate these defects at 300 K and 1 K by setting the maximum thresholds for the distance between the atoms at 3.5 Å and the angles at 10 degrees.

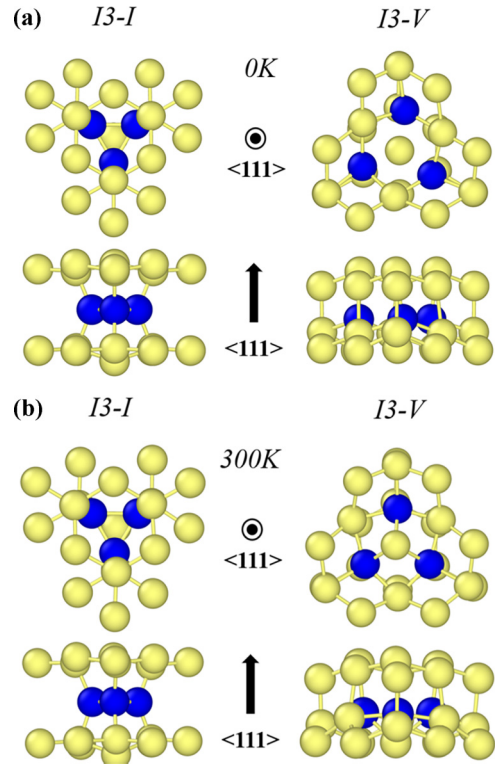


FIG. 2. (a) W-center defect structure candidates, produced by minimization of a distorted tri-interstitial cluster placed in between the {111} planes using the Tersoff potential. W-center with the I3-I (left) and I3-V (right) structure at 0 K. (b) The same defects at 300 K where the average configurations (from 10 different structure snapshots at 300 K) of the clusters are shown. The blue balls correspond to the tri-interstitial defect atoms. Figure created with OVITO software [35].

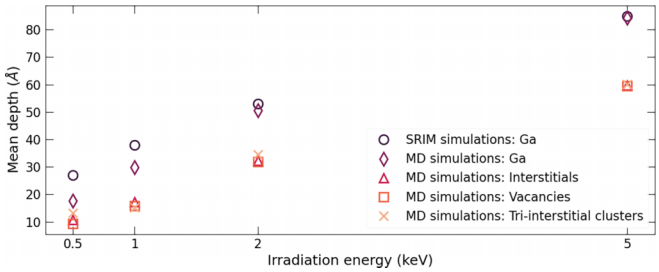


FIG. 3. Ga mean stopping depth and defect mean formation depth as a function of irradiation energy for MD and SRIM simulations.

### B. Irradiation energy and fluence

Next, the effect of irradiation energy and fluence on the formation of defects was studied. In Fig. 3 the mean stopping depth of the Ga atoms and the mean formation depth of interstitials and vacancies identified by the WS analysis as well as the tri-interstitial clusters identified from the developed method are shown for different energies and a fluence of $50 \times 10^{12}$ ions cm$^{-2}$ for one simulation of 50 successively irradiated Ga atoms. The same parameters were employed for SRIM simulations and the ion ranges of Ga atoms are plotted alongside the ones from MD simulations. The two simulation methods give similar results for the Ga mean stopping depth even though no direct comparison can be made between the two methods because of the crystalline and amorphous structures of MD and SRIM, respectively. The MD simulation with 5 keV beam energy exhibits channeling effects, which can be eliminated by a small beam angle of 6°. The defects identified by the WS analysis as well as the tri-interstitial clusters appear to have the same mean depth at each energy which is approximately 2 nm below that of Ga. Their average depth distributions from ten different simulations for the different irradiation energies are shown in Fig. 4. The tri-interstitial clusters are formed near the highly defected region of interstitials and vacancies for the low energies of 0.5 keV and 1 keV, whereas they spread deeper into the sample for the higher energies and especially for the 5 keV, where some tri-interstitial clusters are formed far from the highly defected area (over 100 Å below the surface). The high Ga energies allows them to transfer their energy deeper into the sample and create tri-interstitial clusters in a less distorted environment.

The 5 keV irradiation energy yields the most tri-interstitial clusters deeper into the Si; thus a Ga fluence investigation was carried out for this energy. In Fig. 5 the number of tri-interstitial clusters with the appropriate positioning and orientation (Fig. 5, top) as well as the trigonal symmetric ones (Fig. 5, bottom) are presented for different irradiation fluences. The orange circles for the same fluence represent the number of the clusters produced after a given number of irradiation events for multiple simulations and the black dots the average number over all simulations.

The number of nonsymmetric tri-interstitials appears to increase linearly with the fluence up to $60 \times 10^{12}$ ions cm$^{-2}$, after which it increases more slowly. The trigonal symmetric tri-interstitials reach an approximately stable average after a fluence of $30 \times 10^{12}$ ions cm$^{-2}$ but their number is not sufficient to extract meaningful statistical results. Thus, for the following analysis only the nonsymmetric clusters will be used. Moreover, it is possible that with the appropriate thermal energy a transition can occur from the nonsymmetric to the symmetric tri-interstitial cluster. One possible mechanism for this transition may be the translation and rotation during the diffusion of the clusters which requires relatively small energies [38]. Because of this, the nonsymmetric tri-interstitial clusters can be considered W-center defect candidates.

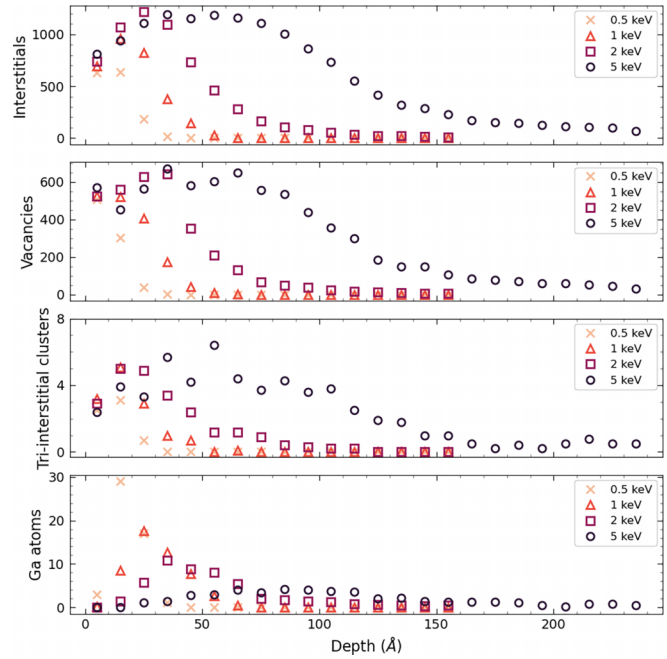


FIG. 4. Interstitials, vacancies, tri-interstitial clusters, and irradiated Ga atom average depth distributions (ten simulations), for different irradiation energies with a fluence of $50 \times 10^{12}$ ions cm$^{-2}$.

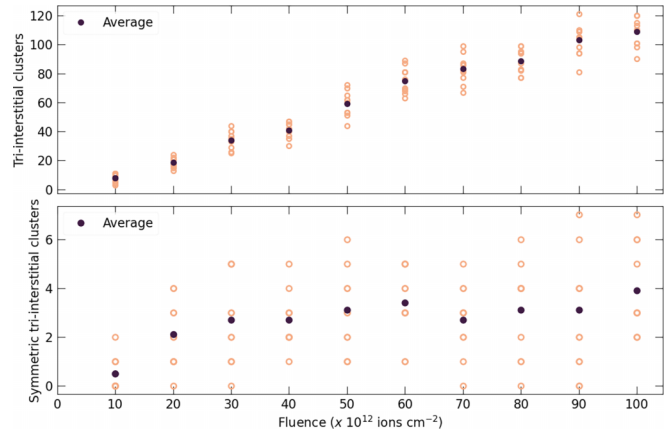


FIG. 5. Nonsymmetric tri-interstitial clusters (top) and symmetric tri-interstitial clusters (bottom) as a function of the irradiation fluence (and irradiated atoms) for 5 keV irradiation energy. The orange circles represent the number of the clusters produced after a given number of irradiation events for multiple simulations and the black dots the average number over all simulations.

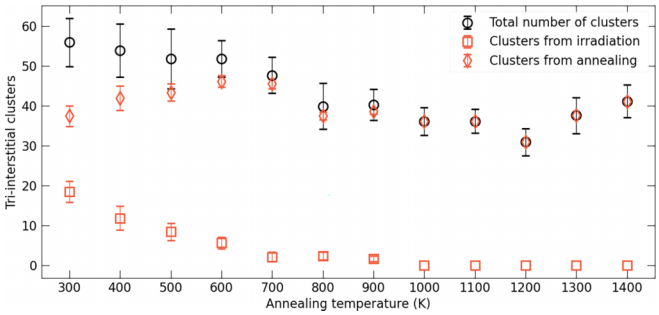


FIG. 6. The number of tri-interstitial clusters after 0.5 ns of annealing at different temperatures for the 5 keV irradiation energy and a fluence of $50 \times 10^{12}$ ions cm$^{-2}$. The black circles represent the total number of tri-interstitial clusters, the orange squares the clusters produced from irradiation, and the orange diamonds the number of clusters produced during annealing.

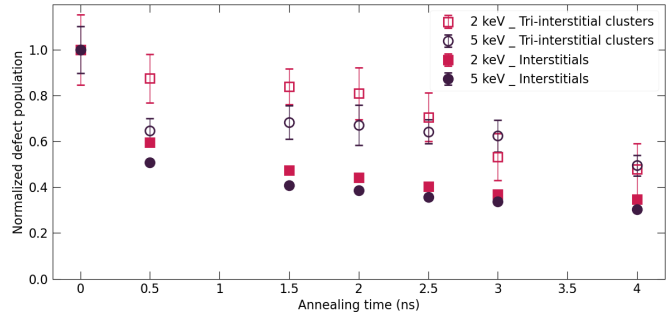


FIG. 7. Normalized number of tri-interstitial clusters and the overall interstitials after different annealing times at 1400 K for different irradiation energies and a fluence of $50 \times 10^{12}$ ions cm$^{-2}$.

### C. Annealing temperature

The annealing temperature is an important parameter [3,7–13] for the formation of silicon emission centers. The MD simulations cannot be used to investigate the full annealing process in terms of time but the trend the defect populations follow during short annealing times can be investigated. Thus, annealing was carried out on the system of 5 keV irradiation energy and a fluence of $50 \times 10^{12}$ ions cm$^{-2}$ for 0.5 ns at different temperatures in the range of 400 K to 1400 K. Figure 6 shows the total number of tri-interstitial clusters after the annealing process alongside the tri-interstitial cluster population that has been produced directly from irradiation and the population produced by the annealing. To estimate the population of clusters produced by irradiation, a computational analysis was performed to assess which tri-interstitial cluster atoms after the annealing are the same as those before the annealing. This can provide an indication on the number of clusters that survive after the annealing process. Accordingly, all the new tri-interstitial cluster atoms identified after the annealing that could not be found after the irradiation are considered to have been produced by the annealing process. The total number of tri-interstitial clusters slowly decreases up to 600 K and then it decreases more rapidly up to 1200 K, from where it increases again. The number of tri-interstitial clusters produced by irradiation decreases with increasing temperature and it becomes practically zero after annealing at temperatures greater than 600 K. This indicates that a lot of the tri-interstitial clusters formed after irradiation are unstable, due to the highly defective areas around them. Thus even small annealing temperatures causes the atoms of such tri-interstitial clusters to diffuse to nearby vacancies or agglomerate with other interstitials. This behavior becomes more prominent as the thermal energy increases. Above 600 K annealing, all the tri-interstitial clusters have been generated by the annealing process. The clusters produced by the annealing process reach a peak value at 600 K after which they start decreasing with annealing temperature until 1200 K. At high annealing temperatures an increase in the number of clusters is observed. This might be attributed to the greater healing of the local environment around potential tri-interstitial clusters, which eventually assists their formation. To conclude, we may say that annealing at low temperatures can create new tri-interstitial clusters and at the same time retain some of the clusters produced during the irradiation process. These results, alongside the overall healing of the environment around the tri-interstitial clusters, may provide a justification of why experimentally low-temperature annealing steps have been shown to enhance the W-center's photoluminescence emission [3,9–12].

### D. Annealing time

The annealing durations of 0.5, 1.5, 2, 2.5, 3, and 4 ns at 1400 K were investigated for systems previously irradiated at all investigated energies with a fluence of $50 \times 10^{12}$ ions cm$^{-2}$. This temperature was selected because it will lead to faster defect evolution and eventually better annihilation of the lattice damage. The normalized average number of interstitials which constitutes unwanted damage to the crystal structure and tri-interstitial clusters can be seen in Fig. 7 for 2 keV and 5 keV irradiated systems. For the smaller energies (not shown) the number of tri-interstitial clusters is small and their annihilation rate is similar to that of the other interstitials. On the contrary for 2 keV and 5 keV irradiated systems the total number of interstitials is reduced with the annealing time falling below 50% after 1.5 ns of annealing whereas the number tri-interstitial clusters only falls below 50% after 4 ns of annealing. Furthermore, the tri-interstitial clusters appear to stabilize, especially for the 5 keV irradiated system in the region 0.5 ns to 3 ns and experience even a small increase at 1.5 ns. This shows that the rate of annihilation of the two types of defects is different, with the number of interstitials reducing quicker than the tri-interstitial clusters. As a consequence, this is an indication that the annealing can eliminate a lot of the unwanted defects, while at the same time keeping the population of the tri-interstitial clusters stable. A visual representation of this can be seen in the defect evolution snapshots of Fig. 8. Apart from the increase of the tri-interstitial clusters to interstitial ratio, it is obvious that a lot of tri-interstitial clusters with less distorted local environment [Fig. 8(b) and Fig. 8(c)] are formed. Before the annealing [Fig. 8(a)] the highly defected environment may have a detrimental effect on the stability of the potential W-centers. Thus, the annealing can further improve the stability and isolation of the tri-interstitial clusters by having a less distorted local environment.

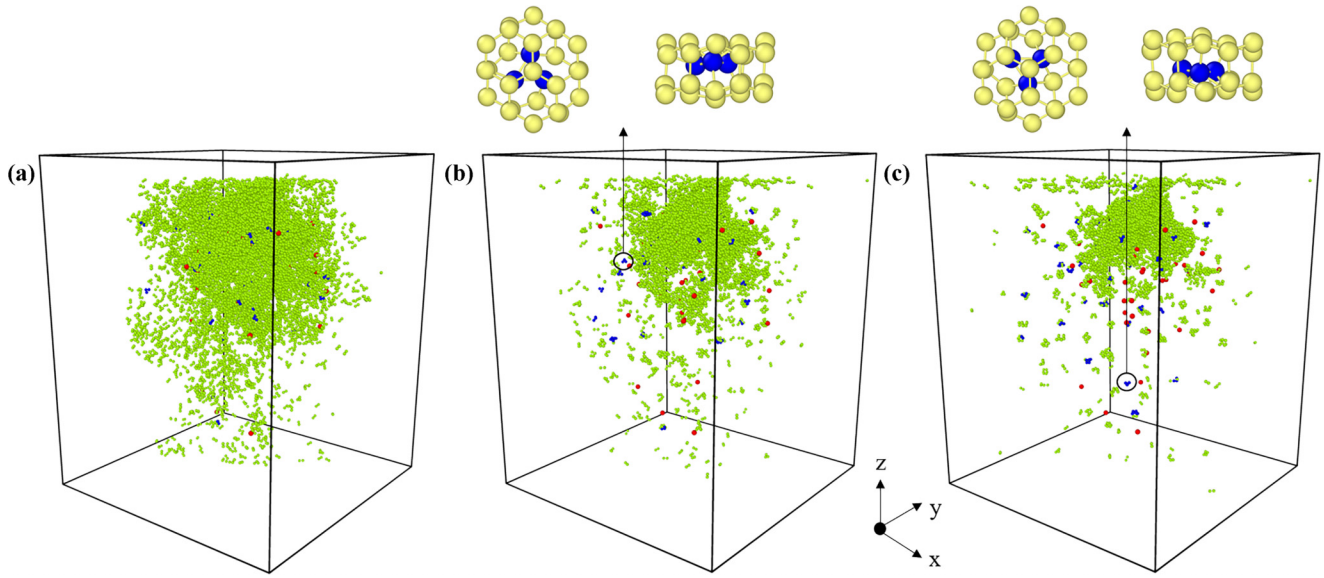


FIG. 8. Snapshots of the defects in the 5 keV irradiation system with a fluence of $50 \times 10^{12}$ ions cm$^{-2}$ (a) before annealing, (b) after 0.5 ns annealing, and (c) 3 ns annealing at 1400 K. The Ga atoms are represented with red, the interstitials with green, and the tri-interstitial clusters with blue. In the black circles and above the simulation box are some of the symmetric tri-interstitials identified by the developed method observed following the ⟨111⟩ (left image) and ⟨11-2⟩ (right image) directions. Figure created with OVITO software [35].

## IV. CONCLUSIONS

In this work molecular dynamics simulations were employed to investigate the formation of W-centers under different, experimentally accessible FIB parameters for Ga irradiation onto Si, as well as the subsequent annealing stage. An identification method was developed to locate potential W-center candidates. It can locate tri-interstitial clusters positioned in between the {111} planes with the appropriate ⟨111⟩ orientation as well as symmetric tri-interstitial clusters which furthermore have trigonal symmetry. The low irradiation energies investigated do not yield many tri-interstitial clusters, which are furthermore concentrated in the highly defected areas. On the other hand, the 5 keV irradiation energy produces more tri-interstitial clusters which are also spread deeper into the Si where the damage is not so severe. The tri-interstitial cluster population increases with the Ga fluence with a decreasing rate whereas the symmetric tri-interstitial clusters appear to stabilize after a fluence of $30 \times 10^{12}$ ions cm$^{-2}$. Low annealing temperatures below 600 K can retain some of the tri-interstitial clusters produced by the irradiation process which, alongside the formation of new clusters at these temperatures, can have a positive impact on the overall population of the tri-interstitial clusters. The annealing for the systems treated with 2 keV and 5 keV irradiation energies showed that the overall interstitial population decreases more rapidly than the tri-interstitial clusters with increasing annealing time. For intermediate annealing times the tri-interstitial clusters in the 5 keV irradiated system appear to stabilize and even increase at some point. This is an indication that the annealing can annihilate a lot of the unwanted defects and at the same time maintain the tri-interstitial clusters which can acquire a better, less distorted local environment. This could lead to more stable and isolated tri-interstitial clusters and, potentially, optically active W-centers. Symmetric tri-interstitial clusters can be found after annealing (top of Fig. 8) but their numbers are not sufficient to extract statistical results. This study hopes to further the understanding of the dynamic formation and evolution of W-centers after FIB irradiation with Ga ions and the subsequent annealing stage and guide future experimental and theoretical work.

## ACKNOWLEDGMENT

We acknowledge financial assistance from the INSA de Lyon "Bonus Qualité Recherche" grant scheme, 2021.

[1] G. Zhang, Y. Cheng, J.-P. Chou, and A. Gali, Material platforms for defect qubits and single-photon emitters, Appl. Phys. Rev. **7**, 031308 (2020).

[2] M. Khoury and M. Abbarchi, A bright future for silicon in quantum technologies, J. Appl. Phys. **131**, 200901 (2022).

[3] G. Davies, E. C. Lightowlers, and Z. E. Ciechanowska, The 1018 meV (W or $I_1$) vibronic band in silicon, J. Phys. C **20**, 191 (1987).

[4] M. Gharaibeh, S. Estreicher, and P. Fedders, Molecular-dynamics studies of self-interstitial aggregates in Si, Phys. B: Condens. Matter **273-274**, 532 (1999).

[5] D. A. Richie, J. Kim, S. A. Barr, K. R. A. Hazzard, R. Hennig, and J. W. Wilkins, Complexity of small silicon self-interstitial defects, Phys. Rev. Lett. **92**, 045501 (2004).

[6] A. Carvalho, R. Jones, J. Coutinho, and P. R. Briddon, Density-functional study of small interstitial clusters in Si: Comparison with experiments, Phys. Rev. B **72**, 155208 (2005).

[7] Y. Baron, A. Durand, P. Udvarhelyi, T. Herzig, M. Khoury, S. Pezzagna, J. Meijer, I. Robert-Philip, M. Abbarchi, J.-M. Hartmann, V. Mazzocchi, J.-M. Gérard, A. Gali, V. Jacques, G. Cassabois, and A. Dréau, Detection of single W-centers in silicon, ACS Photonics **9**, 2337 (2022).

[8] T. Schröder, M. E. Trusheim, M. Walsh, L. Li, J. Zheng, M. Schukraft, A. Sipahigil, R. E. Evans, D. D. Sukachev, C. T. Nguyen, J. L. Pacheco, R. M. Camacho, E. S. Bielejec, M. D. Lukin, and D. Englund, Scalable focused ion beam creation of nearly lifetime-limited single quantum emitters in diamond nanostructures, Nat. Commun. **8**, 15376 (2017).

[9] M. Hollenbach, N. Klingner, N. S. Jagtap, L. Bischoff, C. Fowley, U. Kentsch, G. Hlawacek, A. Erbe, N. V. Abrosimov, M. Helm, Y. Berencén, and G. V. Astakhov, Wafer-scale nanofabrication of telecom single-photon emitters in silicon, Nat. Commun. **13**, 7683 (2022).

[10] P. K. Giri, S. Coffa, and E. Rimini, Evidence for small interstitial clusters as the origin of photoluminescence W band in ion-implanted silicon, Appl. Phys. Lett. **78**, 291 (2001).

[11] G. Davies, S. Hayama, L. Murin, R. Krause-Rehberg, V. Bondarenko, A. Sengupta, C. Davia, and A. Karpenko, Radiation damage in silicon exposed to high-energy protons, Phys. Rev. B **73**, 165202 (2006).

[12] C. Chartrand, L. Bergeron, K. J. Morse, H. Riemann, N. V. Abrosimov, P. Becker, H.-J. Pohl, S. Simmons, and M. L. W. Thewalt, Highly enriched $^{28}$Si reveals remarkable optical linewidths and fine structure for well-known damage centers, Phys. Rev. B **98**, 195201 (2018).

[13] H. Quard, M. Khoury, A. Wang, T. Herzig, J. Meijer, S. Pezzagna, S. Cueff, D. Grojo, M. Abbarchi, H. S. Nguyen, N. Chauvin, and T. Wood, Femtosecond laser induced creation of G and W-centers in silicon-on-insulator substrates, arXiv:2304.03551.

[14] L. Pastewka, R. Salzer, A. Graff, F. Altmann, and M. Moseler, Surface amorphization, sputter rate, and intrinsic stresses of silicon during low energy $Ga^+$ focused-ion beam milling, Nucl. Instrum. Methods Phys. Res., Sect. B **267**, 3072 (2009).

[15] J. Huang, M. Loeffler, W. Moeller, and E. Zschech, Ga contamination in silicon by focused ion beam milling: Dynamic model simulation and atom probe tomography experiment, Microelectron. Reliab. **64**, 390 (2016).

[16] A. V. Rumyantsev, N. I. Borgardt, A. S. Prikhodko, and Y. A. Chaplygin, Characterizing interface structure between crystalline and ion bombarded silicon by transmission electron microscopy and molecular dynamics simulations, Appl. Surf. Sci. **540**, 148278 (2021).

[17] M. F. Russo, M. Maazouz, L. A. Giannuzzi, C. Chandler, M. Utlaut, and B. J. Garrison, Gallium-induced milling of silicon: A computational investigation of focused ion beams, Microsc. Microanal. **14**, 315 (2008).

[18] J. Guénolé, A. Prakash, and E. Bitzek, Atomistic simulations of focused ion beam machining of strained silicon, Appl. Surf. Sci. **416**, 86 (2017).

[19] P. Wang, Q. Chen, Y. Xing, Y. Li, C. Fang, and X. Qiu, Molecular dynamic simulation of orientation-dependent effect on silicon crystalline during sputtering process of focused ion beam, Microsyst. Technol. **25**, 1413 (2019).

[20] Y. Xiao, F. Fang, Z. Xu, and X. Hu, Annealing recovery of nanoscale silicon surface damage caused by Ga focused ion beam, Appl. Surf. Sci. **343**, 56 (2015).

[21] J. F. Ziegler, M. Ziegler, and J. Biersack, SRIM—the stopping and range of ions in matter (2010), Nucl. Instrum. Methods Phys. Res., Sect. B **268**, 1818 (2010).

[22] Y. Fan, Y. Song, Z. Xu, B. Dong, J. Wu, M. Rommel, K. Zhang, J. Zhao, R. Zhu, B. Li, Q. Li, and F. Fang, Molecular dynamics simulation of color centers in silicon carbide by helium and dual ion implantation and subsequent annealing, Ceram. Int. **47**, 24534 (2021).

[23] Y. Fan, Z. Xu, Y. Song, and T. Sun, Molecular dynamics simulation of silicon vacancy defects in silicon carbide by hydrogen ion implantation and subsequent annealing, Diam. Relat. Mater. **119**, 108595 (2021).

[24] Y. Fan, Y. Song, Z. Xu, J. Wu, R. Zhu, Q. Li, and F. Fang, Numerical study of silicon vacancy color centers in silicon carbide by helium ion implantation and subsequent annealing, Nanotechnology **33**, 125701 (2022).

[25] O. Lehtinen, B. Naydenov, P. Börner, K. Melentjevic, C. Müller, L. P. McGuinness, S. Pezzagna, J. Meijer, U. Kaiser, and F. Jelezko, Molecular dynamics simulations of shallow nitrogen and silicon implantation into diamond, Phys. Rev. B **93**, 035202 (2016).

[26] X. Fu, Z. Xu, Z. He, A. Hartmaier, and F. Fang, Molecular dynamics simulation of silicon ion implantation into diamond and subsequent annealing, Nucl. Instrum. Methods Phys. Res., Sect. B **450**, 51 (2019).

[27] W. Zhao, Z. Xu, F. Ren, B. Dong, J. Zhao, and P. Wang, Enhancing the fabrication yield of NV centers in diamond by pre-doping using molecular dynamics simulation, Diam. Relat. Mater. **132**, 109683 (2023).

[28] M. Aboy, I. Santos, P. López, L. A. Marqués, and L. Pelaz, W and X photoluminescence centers in crystalline Si: Chasing candidates at atomic level through multiscale simulations, J. Electron. Mater. **47**, 5045 (2018).

[29] J. Tersoff, Empirical interatomic potential for silicon with improved elastic properties, Phys. Rev. B **38**, 9902 (1988).

[30] A. P. Thompson, H. M. Aktulga, R. Berger, D. S. Bolintineanu, W. M. Brown, P. S. Crozier, P. J. in 't Veld, A. Kohlmeyer, S. G. Moore, T. D. Nguyen, R. Shan, M. J. Stevens, J. Tranchida, C. Trott, and S. J. Plimpton, LAMMPS—a flexible simulation tool for particle-based materials modeling at the atomic, meso, and continuum scales, Comput. Phys. Commun. **271**, 108171 (2022).

[31] J. Tersoff, Modeling solid-state chemistry: Interatomic potentials for multicomponent systems, Phys. Rev. B **39**, 5566 (1989).

[32] A. V. Krasheninnikov and K. Nordlund, Ion and electron irradiation-induced effects in nanostructured materials, J. Appl. Phys. **107**, 071301 (2010).

[33] M. Nakamura, H. Fujioka, K. Ono, M. Takeuchi, T. Mitsui, and M. Oshima, Molecular dynamics simulation of III-V compound semiconductor growth with MBE, J. Cryst. Growth **209**, 232 (2000).

[34] K. Nordlund, S. J. Zinkle, A. E. Sand, F. Granberg, R. S. Averback, R. E. Stoller, T. Suzudo, L. Malerba, F. Banhart, W. J. Weber, F. Willaime, S. L. Dudarev, and D. Simeone, Primary radiation damage: A review of current understanding and models, J. Nucl. Mater. **512**, 450 (2018).

[35] A. Stukowski, Visualization and analysis of atomistic simulation data with OVITO—the Open Visualization Tool, Modell. Simul. Mater. Sci. Eng. **18**, 015012 (2010).

[36] A. F. Wright, Density-functional-theory calculations for the silicon vacancy, Phys. Rev. B **74**, 165116 (2006).

[37] E. R. Batista, J. Heyd, R. G. Hennig, B. P. Uberuaga, R. L. Martin, G. E. Scuseria, C. J. Umrigar, and J. W. Wilkins, Comparison of screened hybrid density functional theory to diffusion Monte Carlo in calculations of total energies of silicon phases and defects, Phys. Rev. B **74**, 121102(R) (2006).

[38] Y. A. Du, S. A. Barr, K. R. A. Hazzard, T. J. Lenosky, R. G. Hennig, and J. W. Wilkins, Fast diffusion mechanism of silicon tri-interstitial defects, Phys. Rev. B **72**, 241306(R) (2005).